Electronic Supplementary Material (ESI) for ChemComm.

Supporting Information

Interface-Induced Fast Li^+ Transport In Mixed Ion–Electronic Conductor

Chenchen He[a], Zhuoxun Zhang[a] and Tao Li[*abc].

[a] Department of Chemistry, Virginia Tech, Blacksburg, VA, 24061, United States.

[b] Department of Chemistry and Biochemistry, Northern Illinois University, DeKalb, Illinois 60115, United States.

[c] X-ray Science Division, Argonne National Laboratory, Lemont, Illinois 60439, United States.

E-mail: tli25@vt.edu.

Experimental

1. Fabrication of anti-perovskite solid electrolyte.

The $Li_2OHCl_{0.75}Br_{0.25}$ (anti-perovskite, AP) was prepared by ball milling and sintering methods as reported previously. First, lithium hydroxide (LiOH, Aladin, >98%), lithium chloride (LiCl sigma-aldrich, >99.95%), and lithium bromide (LiBr Aladin, >99%) with a molar ratio of 1:0.75:0.25 were ball milled (PBM-AD-4L, Deco) at 400 r.p.m. for 2 h. The obtained mixture was placed in a tungsten crucible and transferred to a tube furnace quickly then the tube will be purged into an Ar atmosphere. After two-step heating first to 150°C at the rate of 10 °C min^{-1} for 1 h then to 350°C at the rate of 10 °C min^{-1} for 8 h, the molten products were transferred into Ar-filled glovebox (H_2O<0.1 ppm, O_2<0.1 ppm) and cooled down to room temperature.

2. Sample Preparations

AP–x% CNT (x = 1, 3, 5, 10, and 50 wt.%) composites were prepared by a simple solid-state mixing process. The prepared AP powder and carbon nanotubes (CNT, Sigma Aldrich, 98%) were weighed according to the desired mass ratios. The mixtures were then thoroughly ground in an agate mortar inside an Ar-filled glovebox to ensure homogeneous dispersion of CNT within the AP matrix. The resulting composite powders were collected and stored in the glovebox before further use.

3. Physical Characterization.

High-resolution X-ray powder diffraction (XRD) experiments were performed at the 11-BM-B beamline of the Advanced Photon Source (APS) at Argonne National Laboratory with an average wavelength of 0.4686528 Å. Background contributions from the Kapton capillary tape was subtracted from the data. The Raman spectra of the samples were collected at the Center for Nanoscale Materials, Argonne National Laboratory, using a Renishaw inVia spectrometer with a 532 nm excitation wavelength. The samples were loaded on quartz substrates and sealed with Kapton film to avoid exposure to ambient air. The absorption was measured from the Bromine *K*-edge (13474 eV) and calibrated using a Pb foil prior to data collection by normalization of the pre-edge and post-edge regions. Three transmission scans were averaged for the reported absorption intensity using ATHENA, an open-source package for spectroscopy analysis.

4. Battery assembly.

To assemble the symmetric Li/AP−x% CNT/LPSCl/AP−x% CNT/Li cell, 80 mg LPSCl solid electrolyte powder was pressed into a pellet under 375 MPa in a pellet mold with a diameter of 10 mm. After that, 3–5 mg AP–x% CNT composite was put on both sides of the solid electrolyte and pressed into a pellet. After that, two Li discs with a diameter of 10 mm were attached to both sides of the interlayer. The galvanostatic cycling test was determined by a Land test system (CT2001A). The stack pressure for the symmetric cell was ~25 MPa.

For the Li//AlO@NMC811 full cell, commercial single-crystalline Al_2O_3 coated $LiNi_{0.8}Co_{0.1}Mn_{0.1}O_2$ (AlO@NMC811; MTI, China), as a CAM, and VGCF were vacuum dried overnight at 100°C before mixing the composite cathode. The various composite cathodes were prepared by hand-mixing using an agate mortar at NMC811: LPSCl: VGCF: PTFE weight ratios of 75:20:3:2. To assemble the Li/AP–5% CNT/LPSCl/NMC811 all-solid-state full cells, 80 mg of LPSCl electrolyte was first pressed at 125 MPa to form an electrolyte pellet. Then, 5 mg of composite cathode powder was spread on one side of the electrolyte and AP–5% CNT mixture on the other side and pressed on 375 MPa for 5 minutes. Finally, 20 μm–Li foil was attached to the AP–5% CNT mixture side. Li/AP/LPSCl/NMC811 all-solid-state full cells were assembled in the same methods as Li/AP–5% CNT/LPSCl/NMC811 cells. The stack pressure for the full cell was ~25 MPa. Li/LPSCl/NMC811 full cells without interlayer were also assembled for comparison. To evaluate its cycling characteristics, we evaluated the charging and discharging processes in the constant current mode at a current density of 0.1 C (1 C = 200 mA g^{-1}) and a cut-off of 2.8–4.2 V *vs.* Li/Li^+.

5. Electrochemical measurements.

To evaluate the ionic conductivity of AP-x% CNT (x = 0, 1, 3), the composites were pressed into a pellet under 375 MPa and sandwiched by two stainless steel rods and the Electrochemical impedance spectroscopy (EIS) measurement was performed over the frequency range from 0.1 Hz to 200 kHz at an AC voltage amplitude of 10 mV. The ZView4 program was used to fit the impedance spec. Ionic conductivity of AP-x% CNT (x=5, 10, 50) was obtained from chronoamperometry of Li/LPSC/LNI–50% CNT/LPSC/Li electron-blocking symmetric cells. The applied constant voltage is 10 mV and maintained 60 min. The weight of LPSCl is 50 mg and the resistance contribution from it in both side was estimated to be 100 Ω and was deducted for the calculation of ionic conductivity.

To compare and analyze the electronic conductivity of AP-CNT, we measured the current by chronoamperometry of AP-CNT pellets sandwiched by two stainless steel rods. The measurements maintained 10 min at each step while increasing 0.1 V in the 0.1–0.5 V range for AP-x% CNT (x = 0, 1, 3) and increasing 0.02 V in the 0.02–0.1 V range for AP-x% CNT (x = 5, 10, 50). The current term (I) was averaged for the last 100 points of the measured current value when a constant voltage (V) was applied. The resistance term (R) was calculated using Ohm's law ($R = \Delta V/\Delta I$), and the conductivity value (σ_e) was obtained according to Equation below considering the thickness (l) and area (S) of the pellet.

$$\sigma_e = \frac{l}{RS} = \frac{l}{S} \cdot \frac{\Delta V}{\Delta I}$$

Tafel measurements were performed by recording polarization curves at a scan rate of 0.1 mV s^{-1} from -0.06 V to 0.06 V and the exchange current densities were extracted from the linear fitting of the Tafel regions. All the electrochemical measurements were performed on an electrochemical station (Biologic SP-200).

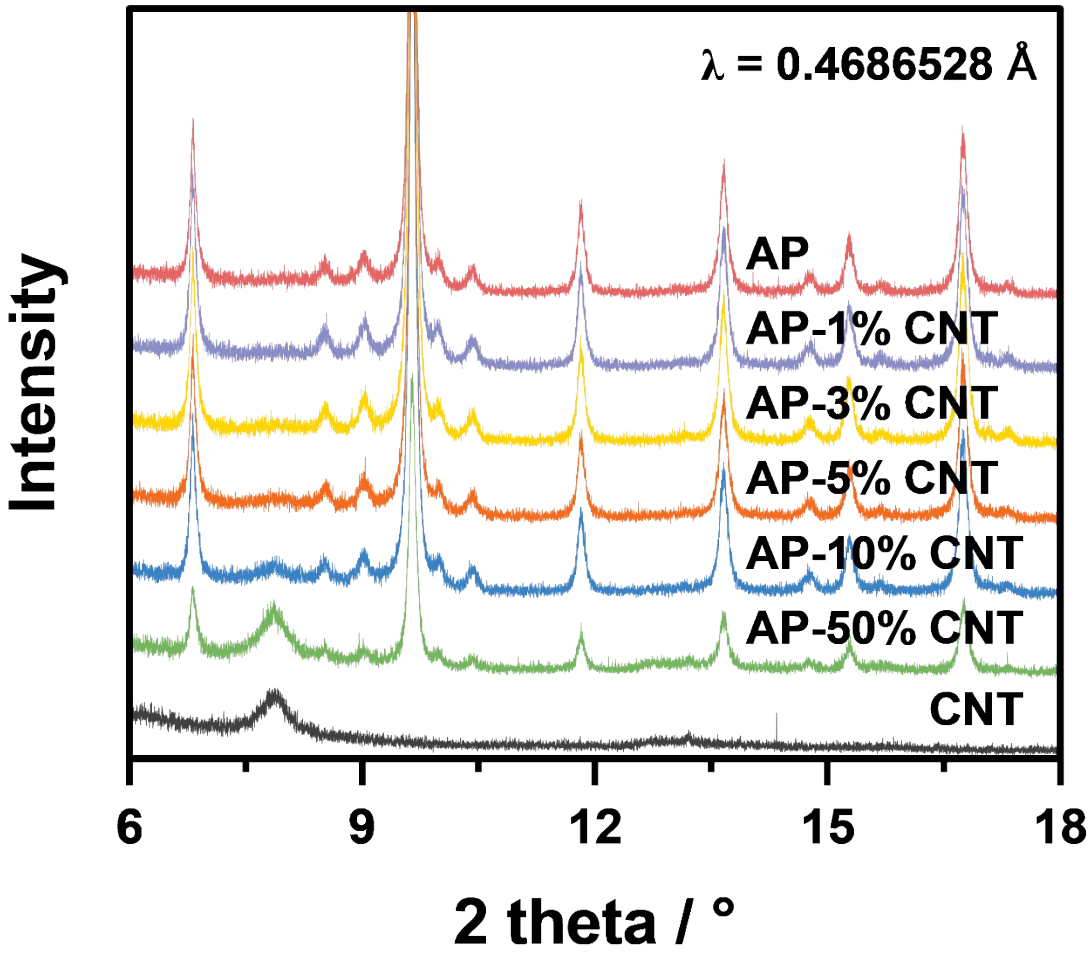

Figure S1. High-resolution X-ray powder diffraction results of AP-x% CNT composite (x=0, 1, 3, 5, 10, 50, 100).

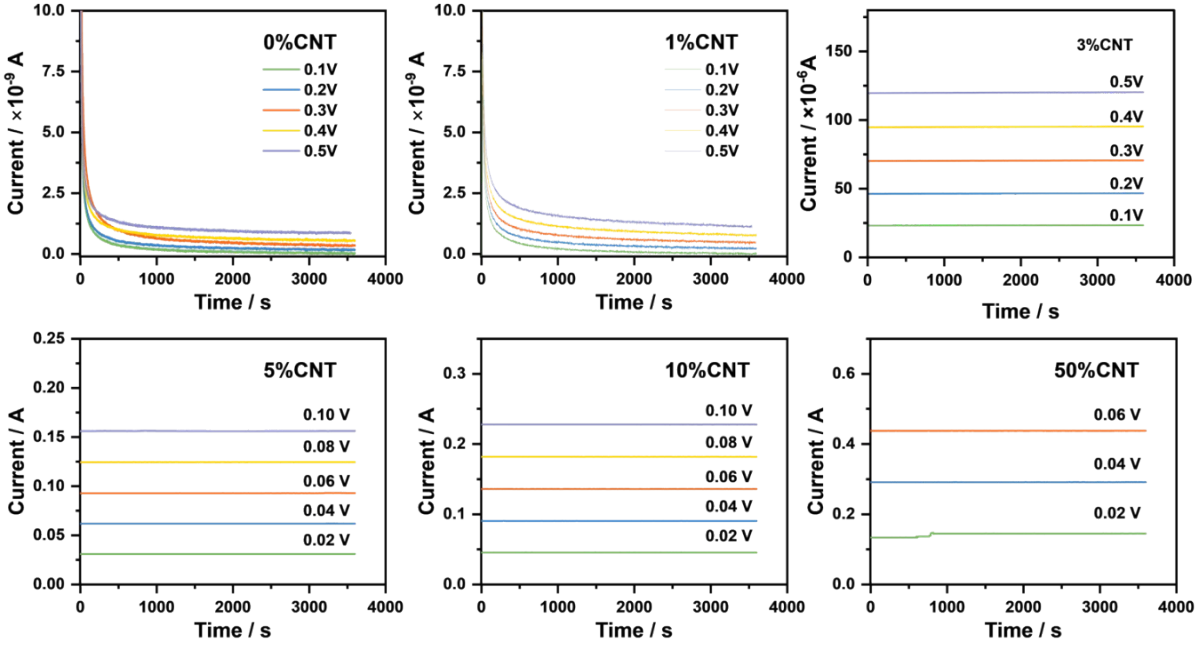

Figure S2. CA measurement of AP-x% CNT (x = 0, 1, 3, 5, 10, 50) with a nonblocking cell of SS/AP-x% CNT/SS cell at 55℃.

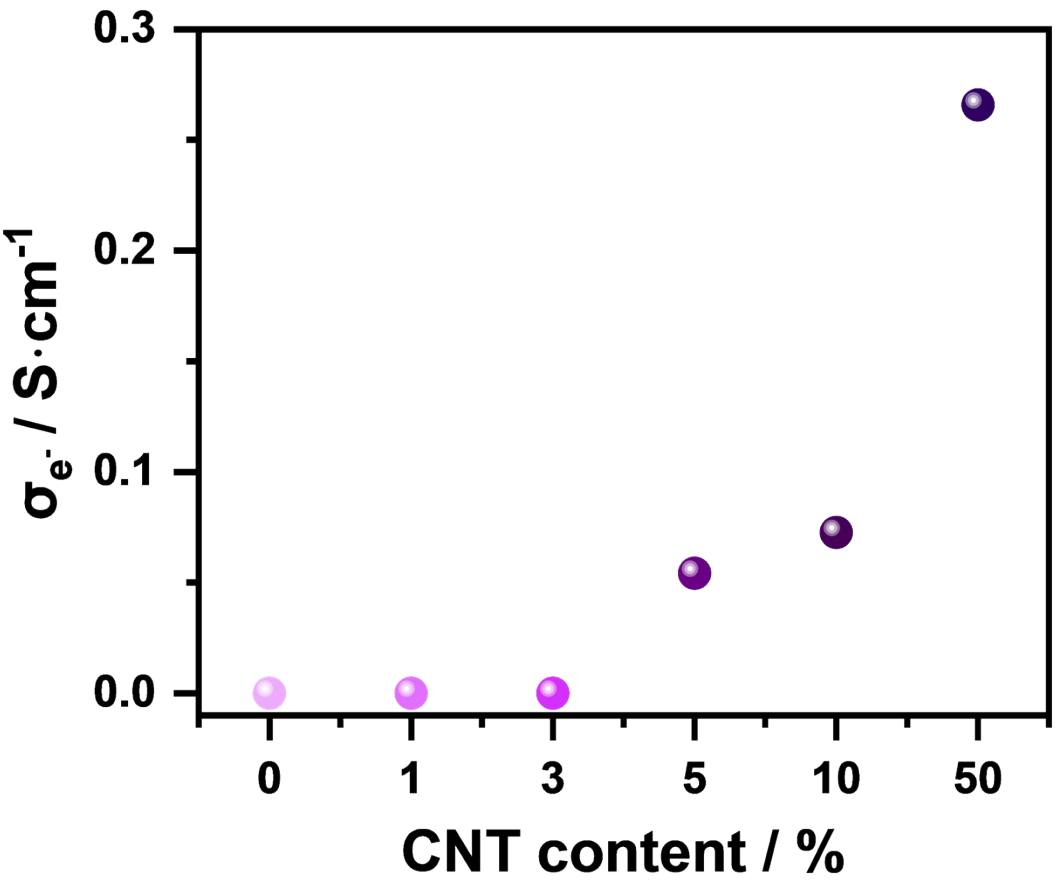

Figure S3. Calculated electronic conductivity of AP-x% CNT (x = 0, 1, 3, 5, 10, 50) from Figure S2.

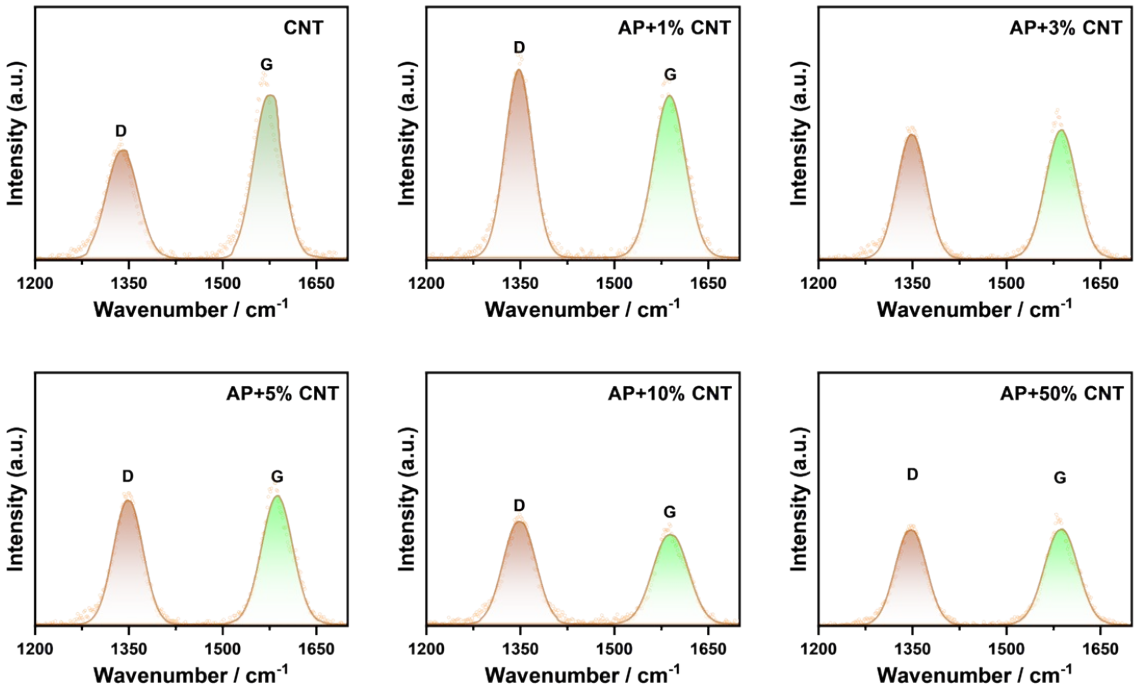

Figure S4. Raman spectra of AP-x% CNT (x = 0, 1, 3, 5, 10, 50).

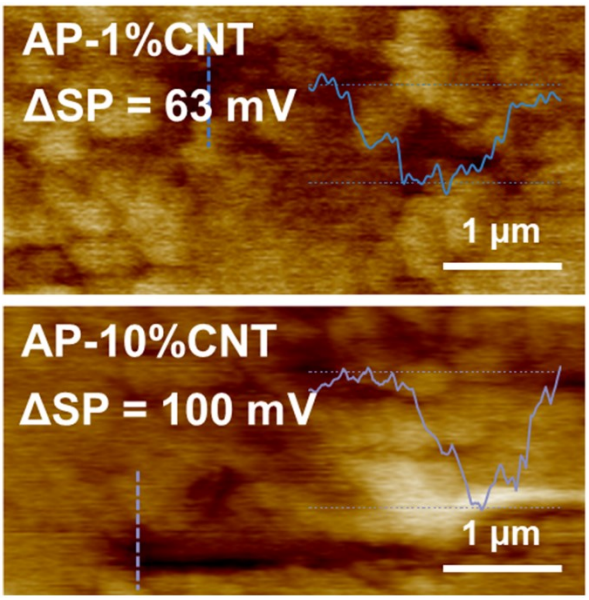

Figure S5. KPFM images and contact potential differences of AP-1%CNT and AP-10%CNT.

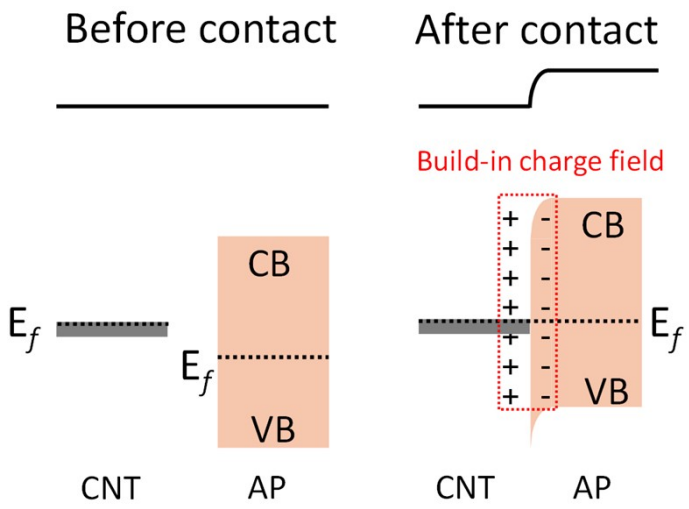

Figure S6. Schematic band diagram illustrating the electronic interaction between AP and CNT before and after contact. Prior to contact, AP and CNT possess distinct Fermi levels and work functions. Upon contact, electrons transfer from CNT to AP until the Fermi levels equilibrate, leading to charge redistribution at the interface. This process results in band bending in the AP phase and the formation of an interfacial built-in electric field across the AP/CNT interface.

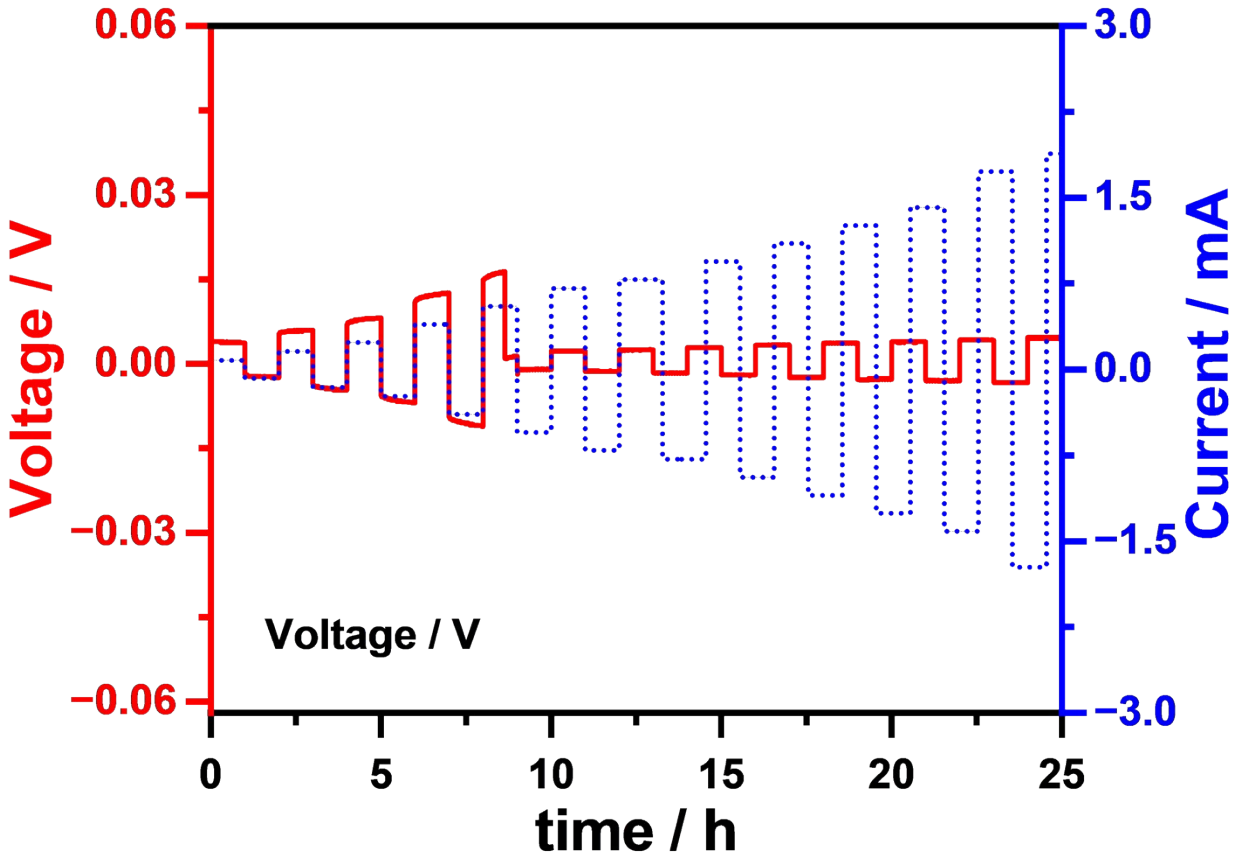

Figure S7. Galvanostatic cycling of Li symmetric cell of Li/LPSCl/Li at step-increased current densities at 55 °C.

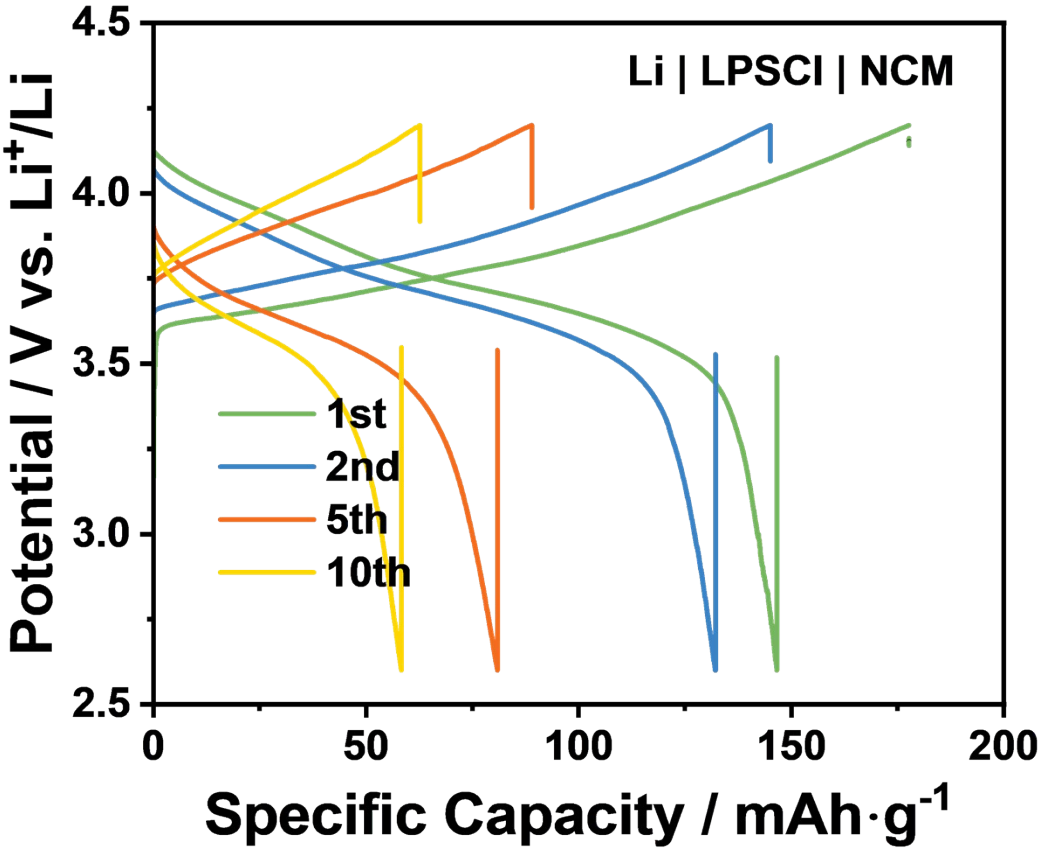

Figure S8. Charge–discharge curves of the Li/LPSCl/NCM811 cell at 55 °C.

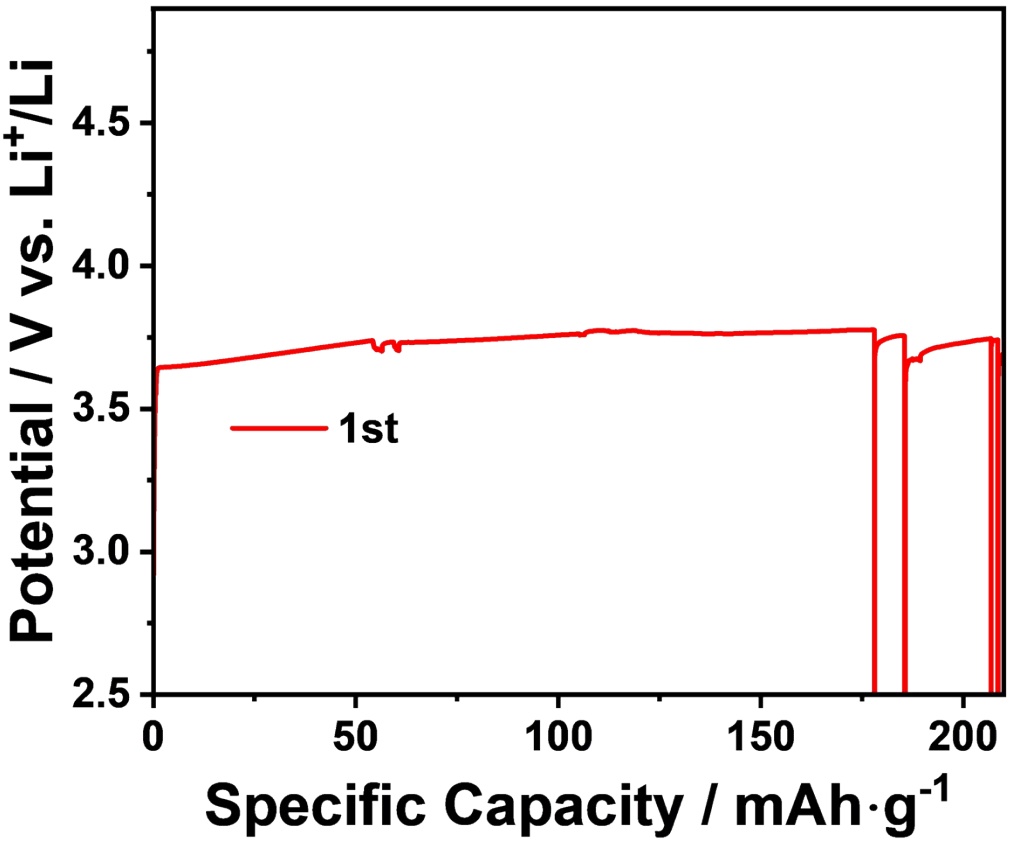

Figure S9. Charge-discharge curve of Li/AP/LPSCl/NCM811 cell at 55 °C.

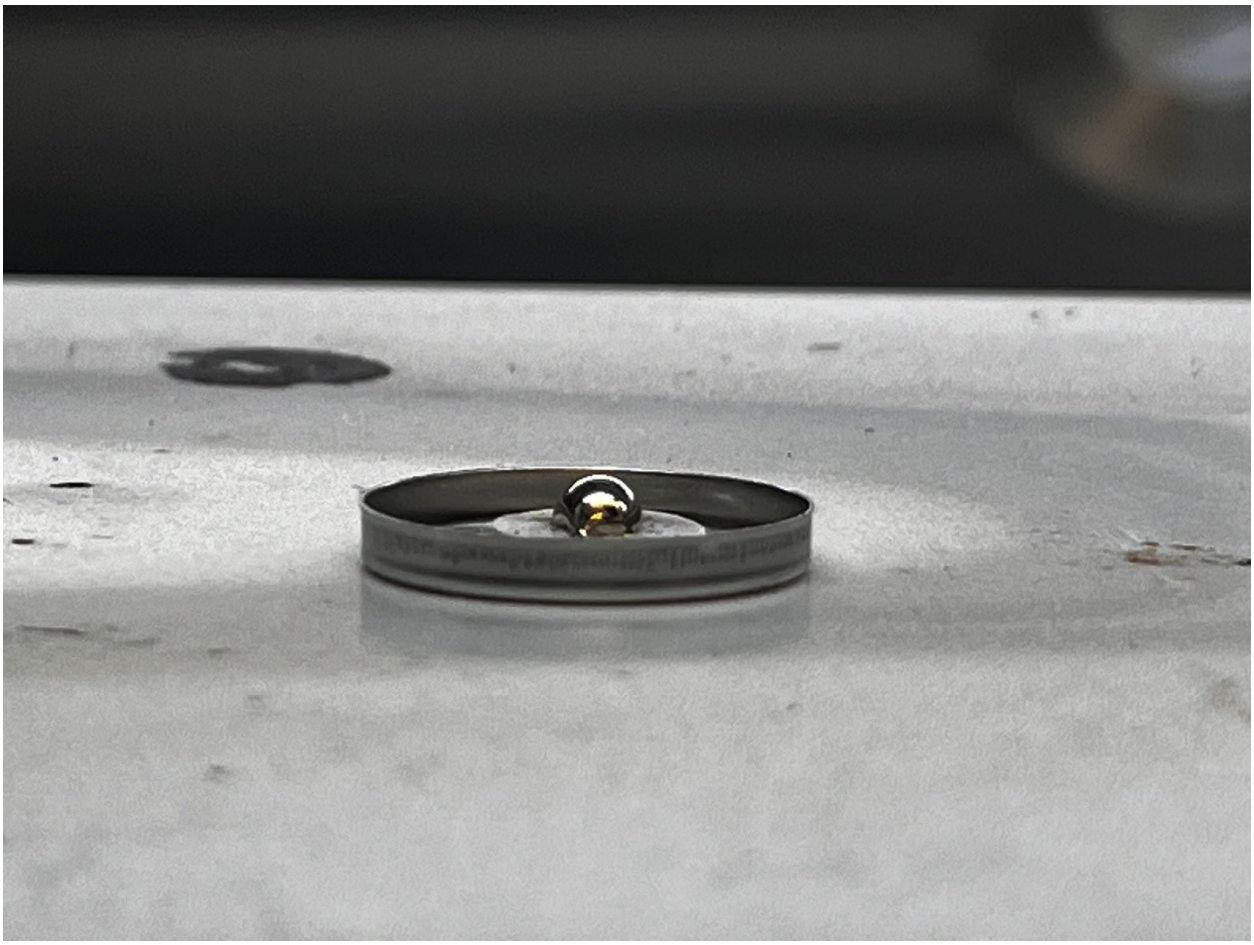

Figure S10. Poor wettability of Li metal on AP pellet.

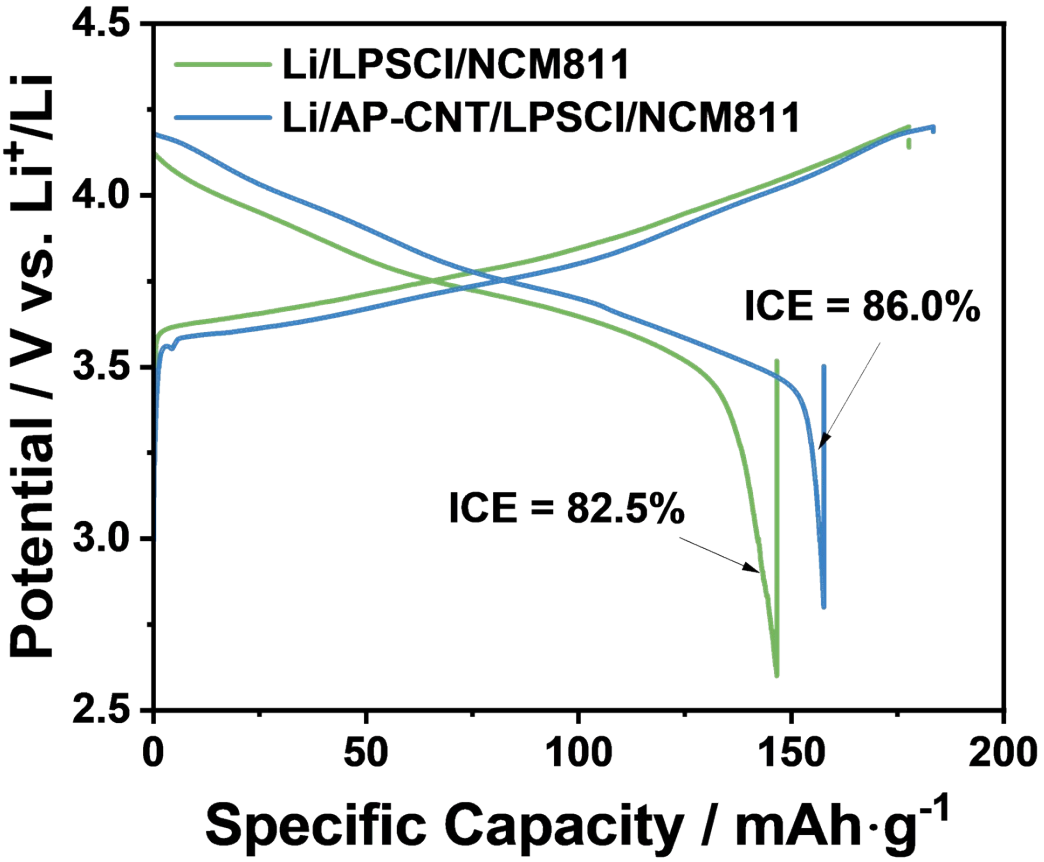

Figure S11. Initial charge–discharge voltage profiles of the ASSLBs with and without AP-CNT interlayer.

Table S1. A summary of Li/SSE interlayer designs, working mechanisms, and electrochemical performance in solid-state batteries

System	Interlayer composition	Key features	CCD (mA cm^{-2})	Full cell lifespan	Ref.
Li/LPSCl/NCM811	Li_3N interlayer	Suppress side reactions	1.9, 50℃	260 cls@80%, 50℃	[1]
Li/LPSCl/NCM811	P_2S_5@Li	In-situ reaction to modulate the surface energy and Li^+ transport	0.4, 25℃	400 cls@75.5%, 25℃	[2]
Li/LPSCl/$LiCoO_2$	Li_3PO_4-Li_3N hybrid interphase	high interface energy and high interfacial adhesion energy	_	80 cls@71.4%, RT	[3]
Li/LPSCl/NCM622	LiF/$LiPO_3$ | LiF/LiAg double layer	Better mechanical contact, LiF improves Li^+ diffusion, reduced nucleation overpotential	2.4, RT	50 cls@96.2%, 60℃	[4]
Li/LPSC/NCM83125	Nano-$AlCl_3$	In-situ reaction to form Li_9Al_4 with high Li diffusivity and lithiophobic LiCl, strain-activated phase separation	2.5, 30℃	300 cls@92.3%, 30℃	[5]
Li/LPSCl/NCM811	Nano ZnO/Gr interlayer	LiC_6 ensures Li^+ transport; interlayer minimize side reactions at the Li/SSEs interface	2.7, 30℃	500 cls@80.9%, 50℃	[6]
Li/LPSCl/NCM811	Ag-C	Separate Li and SSE, Ag reduces Li nucleation energy	_	1000 cls@89%, 60℃	[7]
Li/LPSCl/NCM811	Nano-Sn	Enhance interfacial contact, improve charge transfer kinetics	5.5, 30℃	100 cls@91%, 45℃	[8]
Li/LPSCl/Li	Thin LiPON layer	Conformal interfacial contact, stable against Li	2.7, 30℃	_	[9]
Li/LPSCl/NCM622	LPSCl/LGPS mixed layer	Dynamic stability and lithophilic affinity	1.4, RT	100 cls@93.7%, RT	[10]
Li/LPSCl/NCM811	$Li_2OHCl_{0.75}Br_{0.25}$-CNT	Interface-Induced Fast Li^+ Transport, stable against Li	2.4, 55℃	20 cls@85.0%, 55℃	This work

Reference.

1. P. Ren, X. Wang, B. Huang, Z. Liu and R. Liu, *Journal of Energy Storage*, 2024, **82**, 110200.
2. T. Liu, L. Zhang, J. Li, Y. Li, X. Zhang, K. Lai, S. Zhang, G. Zhao and L. Ci, *J. Power Sources*, 2023, **580**, 233290.
3. H. Su, Y. Liu, Y. Zhong, J. Li, X. Wang, X. Xia, C. Gu and J. Tu, *Nano Energy*, 2022, **96**, 107104.
4. Z. Wu, Z. Jiang, S. Li, Z. Lu, M. Deng, C. Liu, C. Wei, Z. Peng, Z. Wang, L. Zhang and C. Yu, *Nano Energy*, 2025, **138**, 110840.
5. H. Su, J. Li, Y. Zhong, Y. Liu, X. Gao, J. Kuang, M. Wang, C. Lin, X. Wang and J. Tu, *Nat. Commun.*, 2024, **15**, 4202.
6. P. Ren, S. Zhang, B. Li, R. Liu, N. Wu and Y. Li, *Nano Energy*, 2024, **130**, 110127.
7. Y.-G. Lee, S. Fujiki, C. Jung, N. Suzuki, N. Yashiro, R. Omoda, D.-S. Ko, T. Shiratsuchi, T. Sugimoto, S. Ryu, J. H. Ku, T. Watanabe, Y. Park, Y. Aihara, D. Im and I. T. Han, *Nat. Energy*, 2020, **5**, 299-308.
8. G. Kim, S. J. Im, J. H. Yu, C. H. Lee, Y. Son, H. Cha, S. H. Choi, J. S. Yu, J. Hyun, S. Yang, H. Park, J. H. Choi, Y. Kim, Y. C. Ha and K. H. Nam, *Adv. Energy Mater.*, 2026, **16**, e05910.
9. J. Su, M. Pasta, Z. Ning, X. Gao, P. G. Bruce and C. R. M. Grovenor, *Energy Environ. Sci.*, 2022, **15**, 3805-3814.
10. S. Li, S. J. Yang, G. X. Liu, J. K. Hu, Y. L. Liao, X. L. Wang, R. Wen, H. Yuan, J. Q. Huang and Q. Zhang, *Adv. Mater.*, 2024, **36**, e2307768.